Structures of Germanium Clusters: Where the Growth Patterns of Silicon and Germanium Clusters Diverge

Alexandre A. Shvartsburg,[1] Bei Liu,[2] Zhong-Yi Lu,[2] Cai-Zhuang Wang,[2] Martin F. Jarrold,[1] and Kai-Ming Ho[2]
[1]*Department of Chemistry, Northwestern University, 2145 Sheridan Road, Evanston, Illinois 60208*
[2]*Ames Laboratory and Department of Physics and Astronomy, Iowa State University, Ames, Iowa 50011*
(Received 16 February 1999)

We have performed a systematic ground state geometry search for Ge_n neutrals and cations in the $n \leq 16$ size range using density functional theory–local density approximation and gradient-corrected methods. Like their silicon analogs, medium-sized Ge clusters are stacks of tricapped trigonal prism subunits. However, the structures of Ge_n and Si_n for $n = 13$ and $n \geq 15$ differ in details. The onset of the structural divergence between the growth patterns of Si and Ge clusters is confirmed by the measurements of gas phase ion mobilities, fragmentation pathways, and dissociation energies.

PACS numbers: 36.40.Mr

An enormous effort has been invested in the structural characterization of clusters of the group 4 semiconductor elements, silicon and germanium. These are the two most important microelectronics materials, so understanding the growth habit of their clusters is of substantial practical relevance. From an academic viewpoint, cluster research is primarily driven by an interest in the evolution of the structure and properties of materials from the molecular to macroscopic regimes. In the bulk, both Si and Ge pack in a tetrahedral "diamond" lattice. As reviewed below, previous studies of Si_n and Ge_n found that the small clusters (with $n \leq 10$) also have identical geometries. Hence Si and Ge species were expected to be isomorphous in all size regimes. However, ion mobility measurements have revealed a large structural difference between the medium-size clusters of these two elements [1,2]. Si_n^+ clusters grow as prolate structures that rearrange to near-spherical geometries over the $n \sim 24$–30 size range [1], while the near-spherical Ge_n^+ geometries do not appear until $n \sim 65$ [2]. It is important to determine exactly where the growth pathways of Si and Ge clusters diverge and where they converge. We consider the first issue in this contribution.

The structures of Si_n ($n \leq 20$) neutrals and cations have been described [3,4]. We have located the lowest-energy isomers for these species by performing an unbiased global search employing a genetic algorithm and simulated annealing. The energies were calculated using density-functional theory (DFT) in both the local-density approximation (LDA) and gradient-corrected functionals. The resulting structures resemble stacks of particularly stable Si_9 tricapped trigonal prism (TTP) units. The calculated ion mobilities [4], ionization potentials [4], dissociation energies, and fragmentation channels [5] for these geometries are all in excellent agreement with the measurements.

Previous efforts towards the structural characterization of Ge clusters have been less extensive than for silicon (reviewed in Refs. [4,5]) and mostly limited to small sizes ($n \leq 10$). The mass spectra of Si_n and Ge_n appear nearly the same, with "magic numbers" for cations at $n = 4$, 6, and 10 [6,7]. Unlike most other atomic clusters, both Si_n and Ge_n cations [2,5,8] and anions [8] with $n \geq 10$ fragment by fission rather than evaporation, ejecting neutrals with 4–11 atoms. The products of photodissociation [8] and collision-induced dissociation (CID) [2] are almost identical, so dissociation is statistical. Photoelectron spectra (PES) have been recorded for Ge_n anions ($n \leq 32$) [9]. For $n = 3$ and 4, the vibrationally resolved features correspond to triangle and rhombus geometries analogous to those for Si_3^- and Si_4^-. Structural assignments for larger Ge_n^- have been made by modeling the observed electronic transitions [10]. For $n = 5$–9, all bands closely follow those for Si_n^-, which suggests structural isomorphism. Indeed, the optimized geometries for Si_n and Ge_n with $n \leq 10$ are the same [11–16]. The PES for Si_{10}^- and Ge_{10}^- are quite different [9,10]. The global minimum (in LDA) is the C_{3v} tetracapped trigonal prism for Si_{10}^- while the C_{4v} bicapped tetragonal antiprism is the global minimum for Ge_{10}^- [10]. However, the C_{3v} geometry is still the lowest energy one for both neutrals [10]. PES for larger clusters become increasingly featureless, which has prevented structural assignments. The assumed geometries for Ge_n with $n > 10$ have been studied using semiempirical methods only [17]. In summary, there has been no theoretical support for different Si_n and Ge_n geometries at any n.

We have mentioned that mobility measurements for cations show the growth pathways of Si_n and Ge_n to grossly diverge by $n \sim 25$. However, a close examination of the size-dependent trends reveals that the difference occurs by $n = 15$. To pinpoint the onset of this divergence and elucidate the growth of Ge clusters thereafter, we have searched for the lowest energy geometries of Ge_n and Ge_n^+ and compared them with those of the silicon analogs [3,4]. The energies of all isomers were evaluated using LDA and the gradient-corrected Perdew-Wang-Becke 88 (PWB) functional. For silicon, this functional yielded results in excellent agreement with experiment [4,5]. For all calculations, we used the double

numeric basis set with polarization functions as implemented in the all-electron DMOL code [18]. The search for the lowest energy Ge_n geometries was initially attempted by simulated annealing with the Car-Parrinello LDA technique [19], but the geometries produced for $n > 13$ were higher in energy than those obtained by relaxing the Si_n global minima for Ge_n. Clearly, simulated annealing fails to find the lowest energy geometries for Ge_n with $n > 13$, as it failed for Si_n at about the same juncture [3]. We were able to proceed to larger Si_n sizes using a genetic algorithm coupled with a new tight-binding potential. Unfortunately, no such potential presently exists for germanium, and employing a genetic algorithm directly with DFT is computationally prohibitive. So we reoptimized many of the low-energy Si_n isomers for Ge_n. We expect that when the growth pathways of Si and Ge clusters just start to diverge, the Ge_n global minima should be among the low-energy geometries for Si_n. This assumption cannot be verified independently, however the resulting Ge_n structures have been tested against experimental data as discussed below. In any case, for certain sizes the Ge_n geometries are lower in energy than the Si_n global minima relaxed for Ge. This proves the divergence of growth patterns between Si and Ge clusters, even if the above assumption is incorrect.

Our optimized structures for Ge_n with $n \leq 10$ agree with those previously accepted [10–16]. They are the C_{2v} triangle for $n = 3$, D_{2h} rhombus for $n = 4$, D_{3h} trigonal, D_{4h} tetragonal, and D_{5h} pentagonal bipyramids for $n = 5$, 6, and 7, respectively, the C_{2h} distorted bicapped octahedron for $n = 8$, the C_{2v}(I) capped Bernal's structure for $n = 9$, and the C_{3v} tetracapped trigonal prism for $n = 10$. All cases where we found different geometries for Si_n and Ge_n (or Si_n^+ and Ge_n^+) with $n \leq 16$ are listed in Table I. The only difference for $n < 11$ is that the C_1 capped pentagonal bipyramid and the C_{2v}(II) distorted TTP, that are above the global minima by ~0.5 eV for Si_8 and Si_9, respectively [4], become essentially degenerate with them for Ge_8 and Ge_9. For Si_{11}, the C_{2v} isomer of Raghavachari and Rohlfing [20] closely competes with our C_s(I) [4], but for Ge_{11} the C_s(I) isomer is lower by ≈0.35 eV and at least two other geometries are lower than the C_{2v}. The global minimum for Ge_{12} is the same as for Si_{12}: C_{2v} [3,4], while the C_s geometry previously believed to be the ground state for Si_{12} is higher in energy by ≈0.7 eV. The structures of Si and Ge clusters first clearly diverge at $n = 13$: Ge_{13} assumes the C_{2v}(II) structure whereas the C_s isomer, the lowest energy one for Si_{13}, is the third lowest at ≈0.25 eV above the ground state. Si_{14} has only one low-energy isomer, C_s [4], so not surprisingly this geometry is shared by Ge_{14}. The global minimum for Si_{15} is C_{3v}, with less elongated D_{3h}, C_s(I), and C_s(II) [21] isomers ≈0.2 eV higher [4]. For Ge_{15}, the ordering inverts to two isoenergetic structures, C_s(I) and C_s(II), and then near-degenerate D_{3h} and C_{3v} ≈ 0.15 eV higher. The difference between low-energy Si_n and Ge_n geometries increases for $n = 16$: the C_{2h}(II) structure, the global minimum for Si_{16} [4], is ≈0.8 eV above the lowest energy C_{2v} geometry for Ge_{16}, and there are least two other structures in between. The global minima of Si_n and Ge_n for $n = 13$, 15, and 16 are presented in Fig. 1.

TABLE I. Calculated PWB cohesive energies (eV) of selected Si and Ge cluster isomers (with respect to the spin-polarized isolated neutral atoms).

Size	Geometry	Si_n	Si_n^+	Ge_n	Ge_n^+
8	C_{2h}	3.491[a]	2.596[a]	2.103[a]	2.143
8	C_1	3.422	2.596[a]	2.104[a]	2.151[a]
9	C_{2v}(I)	3.580[a]	2.753[a]	3.081[a]	2.305[a]
9	C_{2v}(II)	3.527	2.727	3.082[a]	2.306[a]
9	C_s	3.466	2.690	2.960	2.227
11	C_{2v}	3.618[a]	2.985	3.073	2.469
11	C_s(I)	3.620[a]	3.029[a]	3.105[a]	2.526[a]
11	C_s(II)	3.593	2.973	3.088	2.494
12	C_{2v}	3.648[a]	3.034	3.115[a]	2.543[a]
12	C_s	3.593	3.040[a]	3.060	2.521
13	C_s	3.634[a]	3.093	3.098	2.584
13	C_{2v}	3.616	3.102[a]	3.054	2.575
13	C_{2v}(II)	3.609	3.082	3.118[a]	2.591[a]
15	C_{3v}	3.701[a]	3.225[a]	3.153	2.707
15	D_{3h}	3.688	3.197	3.151	2.701
15	C_s(I)	3.685	3.203	3.162[a]	2.704
15	C_s(II)	3.684	3.219	3.162[a]	2.710[a]
16	C_{2h}(II)	3.672[a]	3.265[a]	3.104	2.701
16	C_{2h}(I)	3.659	3.236	3.091	2.683
16	C_s	3.661	3.240	3.133	2.723
16	C_{3v}	3.642	3.232	3.112	2.720
16	C_{2v}	3.642	3.230	3.157[a]	2.747[a]

[a]Energies of global minima.

We verified the geometries of Si_n neutrals using ionization potential measurements [4]. These are not available for Ge_n. However, ion mobilities, dissociation energies, and pathways are available. All these measurements were performed for cations. The structures of the cations with $n > 5$ have not previously been described, so we reoptimized a number of low-energy Ge_n geometries for Ge_n^+ searching for the global minima. In addition, simulated annealing was performed for $n < 11$. We found that for $n = 5$, 6, 7, and 10, the lowest-energy cation structures are similar to the neutral ground states but Jahn-Teller distorted to lower symmetries: C_{2v} (as also pointed out in Ref. [12]), C_s, C_{2v}, and C_s, respectively. The lowest energy Ge_n^+ with $n \leq 11$ and $n = 14$ are identical to Si_n^+ [4], except that for Ge_8^+ C_1 is clearly preferred to C_{2h} (for Si_8^+ C_1 and C_{2h} are degenerate [4]) and, for Ge_9^+ C_{2v}(I) and C_{2v}(II) are degenerate [for Si_9^+ C_{2v}(I) is preferred]. The lowest-energy Si_{12}^+ assumes a C_s geometry that is different from the C_{2v} neutral [4], but Ge_{12}^+ retains the C_{2v} structure of Ge_{12}. So in the DFT calculations the growth patterns of Si_n and Ge_n cations diverge at $n = 12$, one size earlier than for the neutrals. For $n = 13$, 15, and 16, Si_n^+ and Ge_n^+ are different as they are for Si_n and Ge_n. The global minima for Ge clusters are less sensitive to

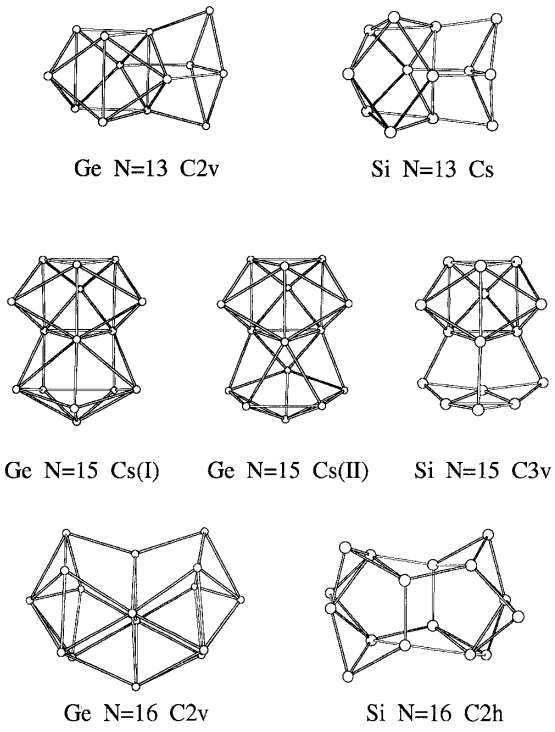

FIG. 1. Lowest-energy geometries (in DFT) for the Si_n and Ge_n neutrals ($n = 13$, 15, and 16).

ionization than those for Si ones, where the energy ordering of isomers for cations and neutrals often differs [4].

The mobilities of Ge_n cations in He gas were measured at two buffer gas temperatures: 78 and 295 K [3,4]. The mobilities for candidate isomers were evaluated by means of trajectory calculations employing a realistic cluster-He potential [22]. This potential was constructed as a sum of Lennard-Jones interactions between the He and each Ge atom plus a charge-induced dipole term that employs the computed partial charges on each atom. This model has been successfully used for Si_n^+ species [3,4]. The elementary LJ interactions were fit to reproduce the measured mobilities of small Ge_n cations with known geometries; the parameters derived were $\varepsilon = 1.50$ meV for the potential depth and $\sigma = 3.45$ Å for the radial extent (the point where the potential becomes zero) [23]. These values are close to those for Si-He potential [4]. Calculated and measured mobilities at 295 K are compared in Fig. 2. The values for the lowest-energy Ge_n^+ geometries described above all agree with the measurements, except for $n = 12$. The agreement between calculations and experiment at 78 K is as good. However, the mobilities for $Ge_{15}^+C_{3v}$ and $Ge_{16}^+C_{2h}$(II), the global minima for Si_{15}^+ and Si_{16}^+, do not match the measurements at either temperature. For Si clusters, these geometries agree with the experiment (but $Si_{15}^+C_s$(I), $Si_{15}^+C_s$(II), and $Si_{16}^+C_{2v}$ do not) [4]. The calculated mobilities for $n \geq 15$ are quite sensitive to the cluster structure. For example, we have located six Ge_{16}^+ isomers within 1 eV from the lowest energy one. Their mobilities at 295 K deviate from the measurement by -2%, $+2\%$, -4.5%, -4.5%, $+2\%$, and -3%. An absolute deviation of $\leq 1\%$ is expected for the correct geometry. So the global minimum for Ge_{16}^+ is the only isomer among at least seven low energy ones to agree with experiment. Unfortunately, the mobilities computed for $Ge_{13}^+C_{2v}$(II) and $Ge_{13}^+C_s$ at either temperature are so close that they could not be distinguished in our experiments. The data do not support the C_{2v} structure for Ge_{12}^+, but the C_s geometry (the global minimum for Si_{12}^+) fits. As for silicon clusters [4], the room-temperature measurements exclude the octahedron-based geometries for Ge_9^+ (C_s tricapped octahedron) and Ge_{10}^+ (T_d tetracapped octahedron). Concluding, the mobility measurements confirm the onset of structural divergence between Si and Ge clusters by $n = 15$ as predicted by the DFT calculations.

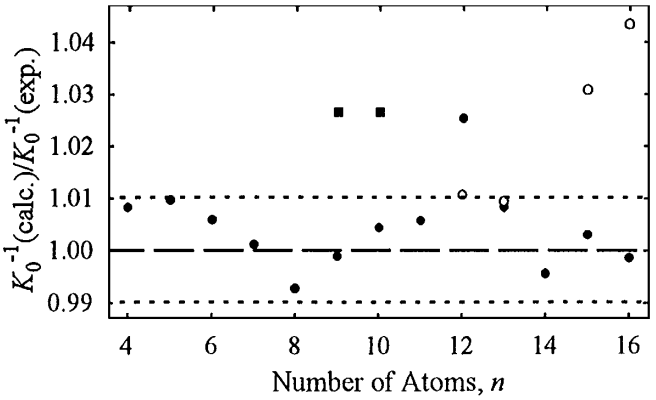

FIG. 2. Relative deviations of the inverse mobilities (K_0^{-1}) calculated for Ge_n cations from the measurements at 295 K. The filled circles are for the lowest-energy isomers, the empty circles are for the geometries that are global minima for Si_n^+, and the squares are for the octahedron-based isomers of Ge_9^+ and Ge_{10}^+ (see text). The dotted lines delimit the error margin of 1%.

Agreement with the mobility measurements is a necessary but not sufficient condition for a structural assignment, because different geometries often have similar mobilities. So it is important to determine directly if the cohesive energies of clusters are fully recovered by calculations. This is accomplished by comparing the computed dissociation pathways and their energies with the experiment [5]. The measured primary fragmentation channels of Ge_n cations ($n \leq 23$) [2] are the same as those for the Si_n^+, except that (i) Ge_9^+ loses Ge while Si_9^+ loses Si_3, and (ii) Ge_{22}^+ and Ge_{23}^+ eject Ge_7 but Si_{22}^+ and Si_{23}^+ eliminate Si_{10}. We have successfully predicted the main fragmentation channels for all Si_n^+ ($n \leq 23$) except Si_{11}^+ using the PWB energies and assuming that the dissociation proceeds along the lowest energy pathway with no activation barrier to reverse process [5]. This model has now reproduced all the primary experimental fragmentation channels for Ge_n^+ up to $n = 23$, *including the changes for* $n = 9$, 22, and 23. The difference in the dissociation of Si_9^+ and Ge_9^+ is not

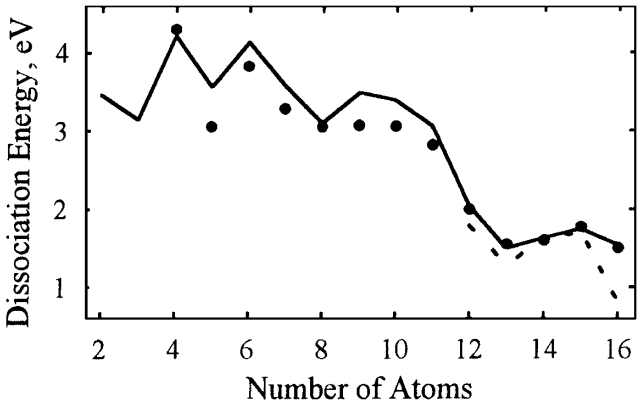

FIG. 3. Dissociation energies of Ge_n cations. The circles are the experimental values [3], and the lines are the PWB calculations. The solid line is for the lowest-energy Ge_n^+ geometries and the dotted line (for $n = 12-16$) is for the isomers that are global minima for Si_n^+.

structurally induced, but that for $n = 22$ and 23 is caused by the different geometries of Si_m^+ and Ge_m^+ for $m = 15$ and 16, respectively. The lower energies of Ge_m^+ relative to Si_m^+ for these sizes make them the preferred products, and this causes the switch in the dissociation channels. If one assumes Ge_{15}^+ (Ge_{16}^+) to have the morphology of Si_{15}^+ (Si_{16}^+), the different dissociation products for $n = 22$ (23) would not be explained.

The fragmentation pattern allows one to verify the relative energies of proposed geometries, but the absolute values are best tested by the dissociation energy measurements. The CID data [2] and our theoretical values are compared in Fig. 3. The agreement is quite good, which proves that our search has, at least, come close to the global minima on Ge_n^+ potential energy surfaces. The dissociation energies calculated for the geometries that are global minima for Si_n^+ ($n = 12$, 13, 15, and 16) (dashed line) are obviously lower than for the geometries optimized for Ge_n^+. For Ge_{16}^+ the difference is probably large enough to disqualify the C_{2h}(II) structure (the difference is somewhat underestimated in Fig. 3 because the DFT dissociation energies are systematically slightly larger than the experimental values). Thus the mobilities, fragmentation pathways, and dissociation energies are all consistent with the structures of Si and Ge clusters being different by $n = 16$.

In summary, we have carried out a systematic ground state geometry search for the Ge_n neutrals and cations with up to 16 atoms. We have found that, like Si clusters, Ge clusters build up by stacking TTP subunits. However, the global minima for certain sizes starting from $n = 13$ differ in details. The theoretical findings for cations are confirmed by the measured gas phase ion mobilities, dissociation energies, and fragmentation pathways.

We thank Professor K. Balasubramanian, Professor J. Chelikowsky, Dr. P. Jackson, and Professor G. Willett for their optimized cluster geometries. This research was supported by the National Science Foundation, the Army Research Office, and the Office of Basic Energy Sciences.

[1] M. F. Jarrold and V. A. Constant, Phys. Rev. Lett. **67**, 2994 (1991).
[2] J. M. Hunter *et al.*, Phys. Rev. Lett. **73**, 2063 (1994).
[3] K. M. Ho *et al.*, Nature (London) **392**, 582 (1998).
[4] B. Liu *et al.*, J. Chem. Phys. **109**, 9401 (1998).
[5] A. A. Shvartsburg *et al.*, Phys. Rev. Lett. **81**, 4616 (1998).
[6] T. P. Martin and H. Schaber, J. Chem. Phys. **83**, 855 (1985).
[7] W. Schulze, B. Winter, and I. Goldenfeld, J. Chem. Phys. **87**, 2402 (1987).
[8] Q. L. Zhang *et al.*, J. Chem. Phys. **88**, 1670 (1988).
[9] O. Cheshnovsky *et al.*, Chem. Phys. Lett. **138**, 119 (1987); G. R. Burton *et al.*, J. Chem. Phys. **104**, 2757 (1996); Y. Negishi *et al.*, Chem. Phys. Lett. **294**, 370 (1998).
[10] J. R. Chelikowsky *et al.*, Mater. Res. Soc. Symp. Proc. **408**, 19 (1996); S. Ögüt and J. R. Chelikowsky, Phys. Rev. B **55**, R4914 (1997).
[11] G. Pacchioni, D. Plavšic, and J. Koutecky, Ber. Bunsenges. Phys. Chem. **87**, 503 (1983); G. Pacchioni and J. Koutecky, J. Chem. Phys. **84**, 3301 (1986).
[12] D. Dai and K. Balasubramanian, J. Phys. Chem. **96**, 9236 (1992); J. Chem. Phys. **96**, 8345 (1992); **105**, 5901 (1996); **108**, 4379 (1998).
[13] P. Jackson *et al.*, Int. J. Mass. Spectrom. Ion. Process. **164**, 45 (1997).
[14] I. Vasiliev, S. Ögüt, and J. R. Chelikowsky, Phys. Rev. Lett. **78**, 4805 (1997).
[15] E. F. Archibong and A. St-Amant, J. Chem. Phys. **109**, 962 (1998).
[16] M. Menon, J. Phys. Condens. Matter **10**, 10 991 (1998).
[17] G. A. Antonio *et al.*, J. Chem. Phys. **88**, 7671 (1988); A. M. Mazzone, Phys. Rev. B **54**, 5970 (1996); P. K. Sitch, T. Frauenheim, and R. Jones, J. Phys. Condens. Matter **8**, 6873 (1996).
[18] DMOL package, 96.0/4.0.0 (MSI, San Diego, 1996).
[19] R. Car and M. Parrinello, Phys. Rev. Lett. **55**, 2471 (1985).
[20] K. Raghavachari and C. M. Rohlfing, Chem. Phys. Lett. **167**, 559 (1990).
[21] For $n = 15$, C_s(II) is identical to the geometry denoted in Ref. [4] as C_1, and C_s(I) is a minor distortion of this structure.
[22] M. F. Mesleh *et al.*, J. Phys. Chem. **100**, 16 082 (1996); A. A. Shvartsburg, G. C. Schatz, and M. F. Jarrold, J. Chem. Phys. **108**, 2416 (1998).
[23] All mobility calculations have been performed for the averages of LDA and PWB geometries. However, the difference in bond lengths is $\sim 1\%$ and the findings are the same with either optimization.